Astronomy & Astrophysics manuscript no. meynadier5992
February 5, 2008
© ESO 2008

arXiv:astro-ph/0610189v1 6 Oct 2006

Low-excitation blobs in the Magellanic Clouds⋆

F. Meynadier[1,2] and M. Heydari-Malayeri[1]

[1] LERMA, Observatoire de Paris, 61 Avenue de l'Observatoire, F-75014 Paris, France
[2] UPMC – Université Paris 6, 4 place Jussieu, 75005 Paris, France

Received .../Accepted ...

ABSTRACT

Aims. We study an unknown, or very poorly known, interstellar H II component in the Magellanic Clouds. This is the first study ever devoted to this class of objects, which we call Low-excitation blobs (LEBs).
Methods. We used low-dispersion spectroscopy carried out at ESO to obtain emission line intensities of Hα, Hβ, and [O III] ($\lambda\lambda$ 4959 + 5007) for 15 objects in the Large Magellanic Cloud and 14 objects in the Small Magellanic Cloud. Results are displayed in excitation ([O III]/Hβ ratio) versus Hβ luminosity diagrams.
Results. We show the presence of an LEB component in the Magellanic Clouds and study its relationship with the already known class of high-excitation blobs (HEBs). The newly found LEBs are lower excitation counterparts of HEBs and are powered by less massive exciting stars. Further study of LEBs is expected to provide new pieces of information for a better understanding the low mass end of the upper initial mass function in the Magellanic Clouds.

Key words. Stars: early-type, – Galaxies: Magellanic Clouds, – ISM: H II regions

1. Introduction

The ionized content of the Magellanic Clouds (MCs) is not limited to giant and supergiant H II regions or to a relatively small number of supernova remnants. Detection of high-excitation H II blobs (hereafter HEBs) showed the presence of an unknown H II component lying mainly adjacent to or toward the typical giant H II regions, and they are rarely in isolation (see Heydari-Malayeri et al. 2002a, and references therein). In contrast to the ordinary H II regions of the MCs, which are extended structures spanning several arcminutes on the sky (> 50 pc) and are powered by a large number of hot stars, HEBs are very dense small regions usually 4″ to 10″ in diameter (1 to 3 pc) affected by local dust. Here we aim at highlighting another almost unknown or very poorly known constituent of the interstellar medium in the MCs, which we call low-excitation blobs (LEBs). So far, no detailed analysis has been devoted to these objects, which outnumber the high-excitation ones although Sanduleak & Philip (1977), in their search for planetary nebulae, presented a list of three low-excitation compact nebulae in the SMC. Similarly, Morgan (1984a) detected six additional objects of this type, which have [O II] λ3727 lines stronger than the Hβ and the doublet of [O III] $\lambda\lambda$4959, 5007 weak compared to Hβ.

The study of LEBs is interesting for several reasons. It sheds light on a genuine ionized component of the interstellar medium in the MCs. Moreover, since LEBs are excited by massive stars of lower temperature/mass, compared with those that power HEBs and typical giant H II regions, investigating them will provide useful information for better understanding the low-mass end of the upper initial mass function. In particular, they hint at the physical conditions necessary for massive star formation in the relatively small molecular clouds that are their likely birth places. Therefore, LEBs represent a thus far ignored interface between several aspects of massive star formation and the interstellar environment.

2. Observations

The observations were performed from 12 to 17 October 1989, with the ESO 1.52m telescope at La Silla (Chile). A Boller & Chivens spectrograph was used with grating #23, which had a dispersion of 114 Å mm^{-1} and ranged in wavelength from 4772 to 6710 Å, centered on 5741 Å. The detector, CCD #13 (type RCA SID 006 EX), had 1024×640 pixels of size 15×15 μm, each pixel corresponding to 0″.68 on the sky; it was binned 2×2 pixels. The resulting data were frames of 515×101 pixels covering ∼ 69″ on the sky along the slit direction. The spatial scales per arcsec for LMC and SMC are 0.24 and 0.32 pc, respectively.

For all objects, we chose an entrance slit of 10″ width in order to secure the whole flux from the object. This was at the expense of degrading the spectral resolution, which was not critical for our purposes. The nights were photometric, and several standard stars were observed each night for flux calibration. Care was taken to center the objects in the middle of the 10″-width slit, in order to ensure the measurement of the whole flux. An example of the spectra is shown in Fig. 1.

Targets were selected from the Henize (1956) catalog on the basis of two criteria: 1) Hα emission, and 2) small angular size (a few arcseconds). Subsequently, a number of them turned out to be planetary nebulae (Table 4), as explained in Sect. 4. It should be underlined that the sample is not complete, mainly

Send offprint requests to: Frédéric Meynadier, Frederic.Meynadier@obspm.fr

⋆ Based on observations obtained at the European Southern Observatory, La Silla, Chile

as far as the LEBs are concerned. Several other fainter LEBs are expected to be present in other MC nebular surveys, for example, Davies et al. (1976). A summary of the observations is listed in Table 1. Some of the objects were observed several times in order to enhance the S/N ratio.

2.1. Data reduction

The data processing from raw images to calibrated 2D spectra was done using standard `iraf` procedures. Flux calibration was performed with 7, 7, 5, 6, 5, and 4 spectrophotometric standard stars respectively for the nights between 12 and 17 October.

A semi-automated `pyraf` task was written in order to retrieve the flux from the 2D data. It allowed us to integrate the flux in each line while defining what zones were usable for background estimation and removing point-like source fluxes. In some cases, that objects did not fit into the 10″ slit may lead to a small under-estimation of the flux in every line.

2.2. Error estimate

The errors involved in the absolute fluxes were estimated assuming a Poisson law for the signal. The S/N, expressed as $F/\Delta F$ where F is the line flux and ΔF the corresponding uncertainty, should be proportional to $\sqrt{N}$, where N represents the number of collected photons. With N itself expressed as $F \times t$ (where t is exposure time), the S/N can therefore be written as:

$$\frac{F}{\Delta F} = k\sqrt{Ft}. \quad (1)$$

The coefficient k is a constant, possibly different for each line, which we determine from the SMC N 81 measurements. This object was observed on three different nights, and for each line (Hα, [O III]λ4959, [O III]λ5007, Hβ) we calculate:

$$k_\lambda = \frac{\sqrt{F_\lambda}}{\Delta F_\lambda \sqrt{t}} \quad (2)$$

where F_λ is the average flux over the three nights, ΔF_λ the spread of the measurements (around 20% of the average flux), and t the mean exposure time. Then, k_λ is used in Eq. 1 to estimate the relative uncertainty on absolute flux measurements for other objects.

Line ratios are more precisely known, because they are (to the first order) insensitive to calibration errors and sky transparency variations from night to night; [O III]/Hβ and Hα/Hβ ratios show only a ∼ 1% variation. To take this fact into account, the error estimate for line ratios was derived from a set of data taken during the same night on LMC N 83B. The data's spread is representative of the non-systematic errors, and we use it to calculate new k_λ coefficients that are adapted to relative photometry error estimates. The uncertainty on the log(LHβ) and [O III]/Hβ values are graphically displayed in Fig. 2 as error bars.

3. Results

The results of flux measurements in various spectral lines are presented in Table 2 for the LMC blobs and Table 3 for the blobs situated in the SMC. Similarly, Table 4 summarizes the results for those objects in both clouds that turned out to be planetary

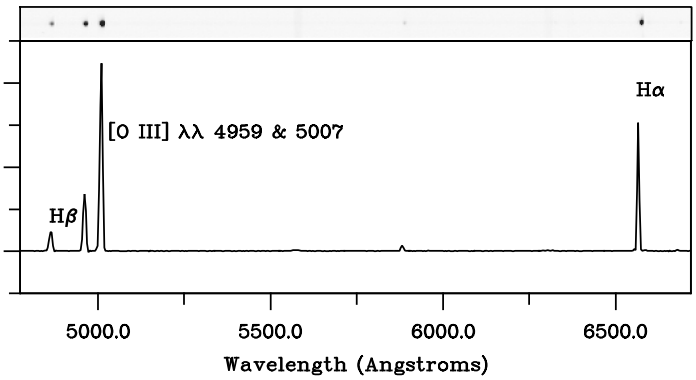

Fig. 1. A sample spectrogram belonging to SMC N 88A. The upper panel shows the 2D spectrum and the lower panel a cut through the central row, with relative intensity scale.

nebulae rather than blobs. In those tables, column 1 lists the object identification according to Henize (1956), column 2 presents the measured uncorrected Hβ flux, and column 3 the sum of uncorrected [O III] line fluxes $\lambda\lambda$4959 + 5007. Column 4 gives the Hα flux, which includes the [NII] doublet $\lambda\lambda$6548, 6584. The logarithmic reddening coefficient at Hβ, based on the Balmer decrement, is presented in column 5; it was derived from comparing the observed Hα/Hβ ratio with the theoretical ratio computed by Brocklehurst (1971) for $T_e = 10^4$ K and $N_e = 10^2$ cm^{-3} under case B conditions. Column 6 lists the de-reddened line ratio [O III] ($\lambda\lambda$4959 + 5007)/Hβ and column 7 the de-reddened Hβ flux. Column 8 gives the Hβ luminosity based on distance moduli of 18.5 mag (Alves 2004) and 19.07 mag (Abrahamyan 2004) for LMC and SMC, corresponding to ∼ 50 and ∼ 65 kpc, respectively. Column 9 lists the diameter of the object in pc, derived from Hα. More specifically, the Hα line profile was integrated into a one-pixel column in the dispersion direction; the result was then fitted by a Gaussian, the FWHM of which yielded the radius. Finally, column 10 presents the average electron densities derived from the formula

$$< N_e >= 5.10 \times 10^4\, D\, R^{-1.5}\, T_e{}^{0.44}\, I(\mathrm{H}\beta), \quad (3)$$

which applies to a Strömgren sphere of pure hydrogen. There, D is the distance in kpc, R the radius in pc, T_e the electron temperature in K (assumed to be 10^4 K), and *I(Hβ)* the nebular flux in units of erg cm^{-2} s^{-1}.

Figure 2 displays the corresponding positions in an excitation/luminosity diagram. The excitation is quantified by the [O III]/Hβ ratio, and the luminosity is derived from the de-reddened Hβ flux. We see that the distribution of SMC points differs from that of LMC data. More specifically, blobs of comparable luminosity tend to be slightly more excited if situated in the SMC. Moreover, several LMC blobs are vertically piled up around a luminosity of 10^{30} W, with [O III]/Hβ ratios ranging from 3.0 to 7.0 (LMC N 160A1, N 11A, N 159, N 83B, N 105A).

The SMC and LMC samples have been fitted by least-square lines, as follows:

– SMC blobs ($\chi^2 = 24.9$):

$$\frac{[\mathrm{O\,III}]}{\mathrm{H}\beta} = 5.1(\pm 0.8)\log(L_{\mathrm{H}\beta}) - 144(\pm 23) \quad (4)$$

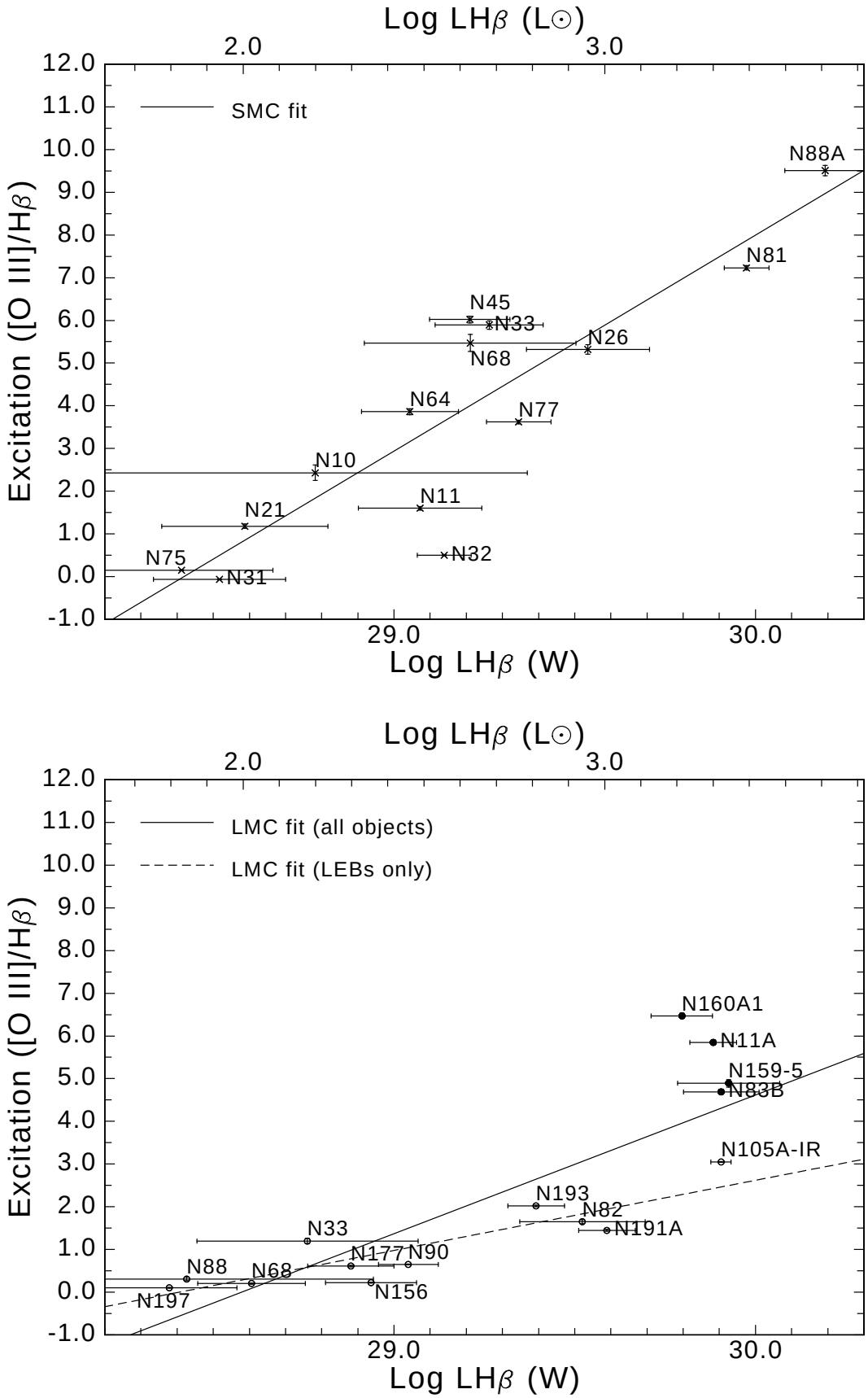

Fig. 2. Excitation (measured by the line ratio [O III] $\lambda\lambda 4959 + 5007$/H$\beta$) versus the H$\beta$ luminosity for the SMC and LMC objects. The logarithmic luminosity scale is in units of watts W, 10^7 erg s^{-1} as well as in units of solar bolometric luminosity. The figures are based on the data presented in Tables 3 and 2, respectively. Solid lines: least-square fits for the SMC and LMC objects. Dashed line: least-square fit for the LMC sample, excluding HEBs (filled dots).

Table 1. Log of observations (exposure times indicated in parenthesis)

Date	LMC objects	SMC objects
12/10	N 11A (2 min), N 160A1 (2 min)	N 9 (5 min), N 11 (2 min), N 77 (5 min), N 81 (5 min)
13/10	N 11A (2 min), N 83B (4×1 min), N 156 (8 min), N 177 (6 min), N 159 (4 min)	N 9 (5 min), N 45 (5 min), N 55 (5 min), N 63 (5 min), N 64 (5 min), N 77 (8 min), N 81 (1 min), N 88A (40 s)
14/10	N 68 (5 min), N 90 (10 min), N 191A (2 min), N 193 (3 min)	N 1 (5 min), N 61 (5 min), N 66 (5 min), N 70 (10 min)
15/10	N 66 (5 min), N 103 (10 min), N 105A-IR (11 min)	N 10 (10 min), N 11(5 min), N 21 (5 min), N 26 (2 min), N 73 (10 min), N 75 (10 min), N 78 (10 min)
16/10	N 33 (5 min), N 44 (2 min), N 66 (5 min), N 68 (5 min), N 82 (1 min), N 88 (1 min), N 197 (10 min)	N 29 (10 min), N 31 (10 min), N 32 (10 min), N 33 (3 min), N 47 (4 min), N 63 (5 min), N 64 (5 min)
17/10	N 6 (20 min), N 11E (5 min), N 159-5 (3 min)	N 68 (5 min), N 81 (1 min), N 88A (1 min)

– LMC blobs ($\chi^2 = 20.0$):

$$\frac{[\mathrm{O\,III}]}{\mathrm{H}\beta} = 3.2(\pm0.6)\log(L_{\mathrm{H}\beta}) - 93(\pm17). \quad (5)$$

The goodness of the SMC fit is affected by N 32: without this point, the χ^2 coefficient falls to 16.6 but the coefficients remain unchanged. On the other hand, fitting the LMC data by a single line is not satisfactory: the vertical accumulation of several blobs around $L(\mathrm{H}\beta) = 10^{30}$ W would suggest dropping them from the least-square fit (see Sect. 4). This leads to the following result:

– Least-square fit for LMC objects, excluding N 160A1, N 11A, N 159-5, and N 83B ($\chi^2 = 1.9$):

$$\frac{[\mathrm{O\,III}]}{\mathrm{H}\beta} = 1.6(\pm0.3)\log(L_{\mathrm{H}\beta}) - 47(\pm9). \quad (6)$$

In both cases, the slope of the SMC fit is significantly steeper than that of LMC. The slope of the second LMC fit (HEBs excluded, Eq. 6) is ∼ 3 times weaker than the slope of the SMC fit (Eq. 4).

4. Discussion

All the sample objects, except one (LMC N 159-5), belong to the renowned Henize (1956) catalog, which presents a collection of the brightest emission nebulae in the MCs. Several surveys searching for planetary nebulae (PNe) have revealed that a small number of the catalog objects are in fact PNe (Jacoby & De Marco 2002; Dopita et al. 1997, and references therein). Therefore, we excluded the known PNe (Table 4) from our sample. Consequently, we are quite confident that the sample of HEBs and LEBs does not contain this type of emission nebulae. As for N159-5 and, similarly, for other HEBs, our previous spectroscopic observations have confirmed their H II region nature (Heydari-Malayeri et al. 1999b, and references therein). Generally speaking, at the distance of MCs, the PNe typically subtend about 1″ on the sky (Dopita et al. 1997; Stanghellini et al. 2002), and our inspection of the size and morphology of the objects in the available images confirm the smaller size and higher compactness of the PNe with respect to the HEBs and LEBs. Note that the PN sizes listed in Table 4 are upper limits, since the binned CCD pixels degrade the profiles of point-like sources. The significantly smaller size and mass of ionized gas are the main reasons that PNe are much less luminous (compare Tables 2 and 3 with Table 4). Thus the brightest PN in the SMC is fainter than intermediate LEBs.

The distribution of the observed objects in the excitation-luminosity space is not quite similar for the LMC and SMC samples (Fig. 2). The whole SMC sample can be readily fitted by a least-square line, as shown in Fig. 2. The LMC objects follow a "straightforward" linear law up to an excitation of $[\mathrm{O\,III}]/\mathrm{H}\beta \sim 3.5$. Approximating the whole LMC sample by a single least-square fit requires justification.

The linear fits are not surprising. In fact, current photoionization models of spherically symmetric H II regions suggest that the $[\mathrm{O\,III}]/\mathrm{H}\beta$ ratio depends on the effective temperature of the star(s), the ionization parameter, and the gas metallicity (Stasińska 1990; Stasińska & Leitherer 1996). The ionization parameter is defined as $U = Q/4\pi R^2 nc$, where Q is the total number of ionizing photons with energy above 13.6 eV, R the Strömgren radius, n the hydrogen density, and c the speed of light. This dimensionless parameter also depends on the volume filling factor via R (Stasińska 2004). Models by Stasińska (1990) show a linear correlation between $[\mathrm{O\,III}]/\mathrm{H}\beta$ and the $\mathrm{H}\beta$ luminosity for H II regions with the same size, the same gas density, and the same number of exciting stars, but with increasing effective temperatures. The reason for this relationship is that as the temperature increases, producing higher $[\mathrm{O\,III}]/\mathrm{H}\beta$ ratios, the value of Q increases as well, increasing the $\mathrm{H}\beta$ luminosity. The models also show that lower metallicity environments favor higher $[\mathrm{O\,III}]/\mathrm{H}\beta$ ratios, but the metallicity dependence can be outweighed by the ionization parameter.

The observed objects in each galaxy have more or less the same physical size and probably the same chemical abundances. Although the gas density can vary from object to object, the observed ascending behavior of the linear fits should mainly be due to increasing stellar temperatures. The scatter around the least-square fits is very likely due to differences in ionization boundedness, density structure, local dust, and age. It should be underlined that this linear behavior is characteristic of H II regions, and planetary nebulae (Table 4) do not follow this trend. In fact, although the planetary nebulae can have higher $[\mathrm{O\,III}]/\mathrm{H}\beta$ ratios, they are all underluminous with respect to H II regions.

Two groups of objects show up in both galaxies. Those populating the upper right parts of the plots are known to be HEBs. These are LMC N 160A1, N 11A, N 159-5, N 83B and SMC N 88A, N 81 (see Heydari-Malayeri et al. 2002a, and references therein). They were called so because of their small size, compactness, and higher $[\mathrm{O\,III}]/\mathrm{H}\beta$ ratio compared to common giant H II regions in the MCs. Here, in light of new observations, it is possible to provide a more precise definition

taking all the data into account. In the LMC sample, an HEB is an object that stands above the linear fit in the [O III]/Hβ-*Log L(Hβ)* space (Fig. 2) and that has a luminosity of *Log L(Hβ)* $\sim$ 30.0 W or *Log L(Hβ)* $\sim$ 3.4 ($L_{\odot}$). This means that an LMC HEB should at the same time have an [O III]/Hβ ratio higher than $\sim$ 4.0. If we use the flatter fit, N 105A-IR can also qualify as an HEB. As regards the SMC HEBs, the "classical" members, N 88A and N 81, fulfill the two criteria specified above. They have at the same time higher excitation compared to the LMC HEBs (see below). Consequently, as a working hypothesis, we call LEBs all the other objects that do not meet the above requirements for excitation and luminosity. Of course one can also consider an intermediate group between the two extreme cases.

As mentioned above, Fig. 2 also shows that the HEBs in the SMC have a higher [O III]/Hβ ratio compared to the LMC sample. This effect is the main reason for a steeper slope of the fit for the SMC population, whether the whole LMC sample is considered or not. This behavior can be explained by the fact that, for the range of metallicities characterizing the MCs, the [O III]/Hβ ratio becomes larger when the metallicity decreases because of the higher temperature of the O^{++} zone (Stasińska 2002). Several observational works hint at an increasing electron temperature gradient with decreasing O abundances as a function of the galactocentric distances (see Deharveng et al. 2000, and references therein). There is also the possibility that low metallicity leads to higher effective temperatures for exciting stars, but the situation is not quite clear (see Martins et al. 2005, for discussion). Observationally, Massey et al. (2004) find higher effective temperatures for SMC O type stars compared to their Galactic counterparts. This is not supported by Heap et al. (2006) and Bouret et al. (2003), who find no temperature difference between O type stars in the SMC and Galaxy. Theoretically, O star atmosphere models by Martins (2005), which take line-blanketing effects into account, show that O stars in the SMC have higher effective temperatures than Galactic stars. This conclusion is supported by Mokiem et al. (2004).

The pile-up behavior of the HEBs in the LMC plot is not clearly understood at this stage. Why is such feature not seen for the SMC HEBs? We note that only two HEBs are present in the SMC plot, implying that, even if this feature existed for the SMC objects, it cannot be shown by the present data. Tentative explanations could be given by taking possible variations in the ionization parameter into account. For example, ionization-boundedness in the HEBs, which are powered by hotter exciting sources or by more numerous sources with the same temperature. Since the HEBs have more or less the same size and, consequently, comparable amounts of matter, the larger Lyman continuum photon fluxes cannot correspondingly create more luminous H II regions. If this explanation is valid, we need to know the physical conditions that give rise to hotter stars or to a larger number of exciting stars, when the available amount of gas in the initial molecular clump is comparable to that in less luminous HEBs. Alternatively, the difference in the density structure/filling factor can result in different [O III]/Hβ ratios while comparable exciting sources are present.

The problem is that the exciting stars of these objects are not well-known. Not only are they generally out of reach of ground-based observations, which lack the necessary angular resolution, even our *HST* observations, obtained using WFPC2, have not been able to resolve them because they are enshrouded in gas and local dust. This is the case for LMC N159-5 (Heydari-Malayeri et al. 1999b) and SMC N88A (Heydari-Malayeri et al. 1999a). As for LMC N160A1 and LMC N83B, one star is detected in each of them (Heydari-Malayeri et al. 2002a, 2001b), but an STIS-like spectrograph is needed to observe them in order to derive their spectral classifications. In the case of N11A, at least 5 stars are detected towards the blob (Heydari-Malayeri et al. 2001a), the main one being an O6 V (Parker et al. 1992). Two stars were detected towards SMC N81 (Heydari-Malayeri et al. 1999c), and subsequent STIS spectroscopy has shown that they have spectral types O6-O8 V (Heydari-Malayeri et al. 2002b; Martins et al. 2004).

Another possibility is the likely presence of dust inside the HEBs. These H II regions are associated with relatively high amounts of local dust, since they harbor newborn massive stars hatching from their parental molecular clouds. Depending on the optical properties of dust grains, photon absorption by internal dust can diminish the Lyman continuum flux as if the exciting source(s) had a lower effective temperature, thus changing the ionization structure of the region. Similarly, the loss of ionizing photons decreases the Hβ luminosity. The presence of internal dust has another implication as far as the extinction correction for the line fluxes is concerned. We used the usual method, which is based on the Balmer decrement measurement, from which the reddening is derived (Howarth 1983). The basic assumption in this method is that the reddening is only due to absorption by the interstellar dust lying on the line of sight. However, this is certainly not true for the HEBs. Therefore, an appropriate extinction correction needs to resolve the radiation transfer equation for a medium in which gas and dust are mixed. Notwithstanding, this is not straightforward since it requires knowing the physical characteristics of the dust grains (Caplan & Deharveng 1986, and references therein). Therefore, the Hβ fluxes can be underestimated.

There is a noteworthy difference between the environments of HEBs and LEBs in the MCs. The HEBs occur mostly in the close vicinity of giant H II regions. In other words, they are generally associated with molecular clouds and regions of active star formation. In contrast, LEBs are isolated objects lying far from giant H II regions, and no conspicuous molecular clouds have been detected to be associated with them. However, the current LEB study suffers dramatically from a lack of data on various aspects of their environment. It would be interesting to find out which environmental conditions give rise to the three different types of H II regions (giants, HEBs, and LEBs) in the MCs. A decreasing scale in the size of the parental molecular cloud may be a decisive factor. But then the question becomes: under which conditions bigger and smaller molecular clouds are formed? We believe that HEBs are younger than giant H II regions and were probably formed from leftover parts of the molecular clouds that brought about the adjacent giant H II regions. The LEBs may be older, evolved HEBs, but appropriate data are needed still to investigate these questions.

Given the difficulty in observing the MC HEBs and LEBs, it would be helpful to study similar objects in our Galaxy for which higher resolution observations are possible. First it should be underlined that HEBs and LEBs are particularly important in the context of massive star formation in the MCs. To our knowledge, no studies have been undertaken yet to find and study com-

pact H II regions in the vicinity of Galactic giant H II regions. As a first step in Galactic work, it would seem helpful to identify this type of Galactic object to compare the physical properties of higher and lower excitation compact H II regions of comparable sizes. Such a study will undoubtedly constitute a research project on its own, to which enough time and effort should be devoted. However, we see two notable handicaps: distance uncertainties involved in Galactic H II region studies and the difficulty of measuring the total luminosity of Galactic objects extending over several arcminutes on the sky. What can be said at this stage is that Galactic H II regions like Orion, Sh2-156, Sh2-152, Sh2-269, and RCW34 (Simpson 1973; Heydari-Malayeri et al. 1980; Heydari-Malayeri & Testor 1981; Heydari-Malayeri et al. 1982; Heydari-Malayeri 1988) have the same physical size and excitation as the MC LEBs. It remains to identify their higher excitation counterparts in the peripheral zones of giant H II regions.

Acknowledgements. We are grateful to Dr. Grażyna Stasińska, of the Paris Observatory/CNRS, for helpful discussions and comments. We would also like to thank an anonymous referee for remarks and suggestions that helped improve the paper.

References

Abrahamyan, H. V. 2004, Astrophysics, 47, 18
Alves, D. R. 2004, New Astronomy Review, 48, 659
Bouret, J.-C., Lanz, T., Hillier, D. J., et al. 2003, ApJ, 595, 1182
Brocklehurst, M. 1971, MNRAS, 153, 471
Caplan, J. & Deharveng, L. 1986, A&A, 155, 297
Davies, R., Eliott, K., & Meaburn, J. 1976, Mem. R. Astron. Soc., 81, 89
Deharveng, L., Peña, M., Caplan, J., & Costero, R. 2000, MNRAS, 311, 329
Dopita, M. A., Vassiliadis, E., Wood, P. R., et al. 1997, ApJ, 474, 188
Heap, S. R., Lanz, T., & Hubeny, I. 2006, ApJ, 638, 409
Henize, K. G. 1956, ApJS, 2, 315
Heydari-Malayeri, M. 1988, A&A, 202, 240
Heydari-Malayeri, M., Charmandaris, V., Deharveng, L., et al. 2002a, A&A, 381, 941
Heydari-Malayeri, M., Charmandaris, V., Deharveng, L., et al. 2001a, A&A, 372, 527
Heydari-Malayeri, M., Charmandaris, V., Deharveng, L., et al. 2001b, A&A, 372, 495
Heydari-Malayeri, M., Charmandaris, V., Deharveng, L., Rosa, M. R., & Zinnecker, H. 1999a, A&A, 347, 841
Heydari-Malayeri, M., Rosa, M. R., Charmandaris, V., Deharveng, L., & Zinnecker, H. 1999b, A&A, 352, 665
Heydari-Malayeri, M., Rosa, M. R., Schaerer, D., Martins, F., & Charmandaris, V. 2002b, A&A, 381, 951
Heydari-Malayeri, M., Rosa, M. R., Zinnecker, H., Deharveng, L., & Charmandaris, V. 1999c, A&A, 344, 848
Heydari-Malayeri, M. & Testor, G. 1981, A&A, 96, 219
Heydari-Malayeri, M., Testor, G., Baudry, A., Lafon, G., & de La Noe, J. 1982, A&A, 113, 118
Heydari-Malayeri, M., Testor, G., & Lortet, M. C. 1980, A&A, 84, 154
Howarth, I. D. 1983, MNRAS, 203, 301
Jacoby, G. H. & De Marco, O. 2002, AJ, 123, 269
Martins, F. 2005, PhD thesis, Université Paul Sabatier, Toulouse
Martins, F., Schaerer, D., & Hillier, D. J. 2005, A&A, 436, 1049
Martins, F., Schaerer, D., Hillier, D. J., & Heydari-Malayeri, M. 2004, A&A, 420, 1087
Massey, P., Bresolin, F., Kudritzki, R. P., Puls, J., & Pauldrach, A. W. A. 2004, ApJ, 608, 1001
Meyssonnier, N. & Azzopardi, M. 1993, A&AS, 102, 451
Mokiem, M. R., Martín-Hernández, N. L., Lenorzer, A., de Koter, A., & Tielens, A. G. G. M. 2004, A&A, 419, 319
Morgan, D. H. 1984a, MNRAS, 209, 241
Morgan, D. H. 1984b, MNRAS, 208, 633
Parker, J. W., Garmany, C. D., Massey, P., & Walborn, N. R. 1992, AJ, 103, 1205
Peña, M., Hamann, W.-R., Ruiz, M. T., Peimbert, A., & Peimbert, M. 2004, A&A, 419, 583
Sanduleak, N., MacConnell, D. J., & Philip, A. G. D. 1978, PASP, 90, 621
Sanduleak, N. & Philip, A. G. D. 1977, PASP, 89, 792
Simpson, J. P. 1973, PASP, 85, 479
Stanghellini, L., Shaw, R. A., & Mutchler, M. 2002, in Revista Mexicana de Astronomia y Astrofisica Conference Series, ed. W. J. Henney, J. Franco, & M. Martos, 112–116
Stasińska, G. 1990, A&AS, 83, 501
Stasińska, G. 2002, in Revista Mexicana de Astronomia y Astrofisica Conference Series, ed. W. J. Henney, J. Franco, & M. Martos, 62–69
Stasińska, G. 2004, in *Cosmochemistry. The melting pot of the elements*, ed. C. Esteban, R. J. García López, A. Herrero, & F. Sánchez (Cambridge University Press), 115–170
Stasińska, G. & Leitherer, C. 1996, ApJS, 107, 661
Walker, A. R. 1983, MNRAS, 203, 25

Table 2. LMC line measurement results

Object LMC	F(Hβ) 10^{-16} W / m^2	[O III] 4959+5007 10^{-16} W / m^2	Hα 10^{-16} W / m^2	c(Hβ)	[O III]/ Hβ	I(Hβ) 10^{-16} W / m^2	L(Hβ) 10^{26} W	radius pc	<Ne> cm^{-3}
N 11A	85.8	518.0	339.7	0.46	5.85	253.0	7638	0.7	1170
N 33	1.6	2.1	9.9	1.07	1.20	19.1	576	0.2	1650
N 68	6.7	1.4	23.7	0.30	0.20	13.4	404	1.3	110
N 82	24.5	42.3	110.6	0.65	1.65	109.9	3319	0.2	4260
N 83B	66.6	326.8	290.5	0.60	4.69	266.4	8043	0.3	3710
N 88	3.4	1.1	13.0	0.42	0.31	8.8	267	1.0	130
N 90	10.6	7.2	44.0	0.54	0.65	36.3	1096	1.4	160
N 105A-IR	84.9	268.6	344.0	0.50	3.05	265.9	8028	1.1	690
N 156	5.7	1.3	26.7	0.70	0.22	28.6	863	1.0	240
N 159-5	11.8	63.9	88.5	1.37	4.89	279.3	8431	0.6	1600
N 160A1	50.7	342.9	222.6	0.61	6.47	207.1	6253	0.6	1530
N 177	8.6	5.4	34.1	0.47	0.61	25.2	760	0.8	320
N 191A	60.2	89.2	216.9	0.33	1.45	128.6	3883	0.7	960
N 193	39.9	82.5	142.0	0.31	2.02	81.9	2472	0.9	500
N 197	2.1	0.2	9.1	0.57	0.10	7.9	239	1.0	130

Table 3. SMC line measurement results

Object SMC	F(Hβ) 10^{-16} W / m^2	[O III] 4959+5007 10^{-16} W / m^2	Hα 10^{-16} W / m^2	c(Hβ)	[O III]/ Hβ	I(Hβ) 10^{-16} W / m^2	L(Hβ) 10^{26} W	radius pc	<Ne> cm^{-3}
N 10	2.7	7.0	12.3	0.64	2.43	11.9	605	3.0	40
N 11	9.1	14.7	34.5	0.40	1.60	23.2	1180	1.0	270
N 21	2.9	3.5	11.1	0.42	1.18	7.6	387	0.6	360
N 26	12.7	71.2	60.4	0.73	5.32	67.8	3440	0.5	1350
N 31	2.2	-0.1	8.8	0.46	-0.06	6.5	329	0.4	660
N 32	13.1	6.7	46.8	0.32	0.50	27.1	1377	1.4	190
N 33	11.0	67.6	45.3	0.51	5.89	36.1	1834	0.5	920
N 45	11.9	73.9	45.9	0.43	6.02	31.9	1621	1.4	190
N 64	8.2	32.8	31.7	0.42	3.86	21.8	1107	1.5	150
N 68	1.8	10.6	12.2	1.26	5.47	32.0	1625	0.4	1380
N 75	1.2	0.2	5.3	0.63	0.15	5.1	259	2.6	30
N 77	14.9	55.7	59.1	0.47	3.62	43.6	2214	1.7	180
N 81	124.9	915.4	403.3	0.17	7.23	186.1	9451	1.1	750
N 88A	88.0	871.7	368.5	0.54	9.51	307.1	15594	0.5	2620

Table 4. Objects excluded from the HEB/LEB sample

Object	F(Hβ) 10^{-16} W / m^2	[O III] 4959+5007 10^{-16} W / m^2	Hα 10^{-16} W / m^2	c(Hβ) 10^{-16} W / m^2	[O III]/ Hβ	I(Hβ) 10^{-16} W / m^2	L(Hβ) 10^{26} W	radius pc	Notes
Planetary Nebula, LMC :									
N 66	3.5	40.2	11.4	11.37	0.17	5.2	157	0.3	(a) (b)
Symbiotic star, SMC :									
N 73	0.7	0.1	7.2	0.20	1.89	51.5	2615	0.3	(c)
Planetary Nebulae, SMC :									
N 1	2.5	9.1	9.8	3.64	0.45	7.1	361	0.3	(d)
N 9	18.0	69.3	51.6	3.84	0.00	18.1	917	0.7	(e)
N 29	0.3	1.8	1.3	6.29	0.60	1.2	60	0.3	(d)
N 47	3.9	16.3	12.4	4.18	0.15	5.5	280	0.3	(d)
N 61	10.0	22.4	35.7	2.25	0.31	20.6	1047	0.5	(f)
N 70	2.9	18.1	11.7	6.24	0.50	9.1	462	0.2	(d)

(a) (Peña et al. 2004). (b) Morgan (1984b) (c) (Walker 1983) (d) Sanduleak et al. (1978) (e) Meyssonnier & Azzopardi (1993) (f) Jacoby & De Marco (2002)